Analyst

Accepted Manuscript

This article can be cited before page numbers have been issued, to do this please use: H. Song, G. Gao, C. Ma, Y. Li, J. Shi, X. Zhou and Z. Zhu, *Analyst*, 2020, DOI: 10.1039/D0AN00880J.

ROYAL SOCIETY OF CHEMISTRY

rsc.li/analyst

ROYAL SOCIETY OF CHEMISTRY View Article Online
DOI: 10.1039/D0AN00880J

Journal Name

ARTICLE

A Hybrid System Integrating Xylose Dehydrogenase and NAD+ coupled with PtNPs@MWCNTs Composite for Real-Time Biosensing of Xylose

Received 00th January 20xx,
Accepted 00th January 20xx

DOI: 10.1039/x0xx00000x

www.rsc.org/

Haiyan Song[a,#], Guangheng Gao[b,#], Chunling Ma[a,#], Yunjie Li[a], Jianguo Shi[c], Xigui Zhou[a], Zhiguang Zhu[a,c,*]

The wide application of xylose in food, beverage, pharmaceutical industries, as well as in the booming field of biorefinery, calls for the demand of a rapid, accurate, and real-time xylose sensing technique rivaling with conventional methods based on chromatography, spectroscopy, and electrochemical analysis using non-specific enzymes or abiotic catalysts. Herein, a hybrid system comprising of polyethylene glycerol swing arm-tethered NAD+ and xylose dehydrogenase (XDH), coupled with platinum nanoparticles deposited on carbon nanotubes (PtNPs@MWCNTs), was constructed for real-time sensing of xylose. The use of PtNPs@MWCNTs composite enhanced the sensitivity of electric response and reduced the oxidation potential of NADH significantly. Further, the NAD+ immobilization allowed for the increase of its microenvironment concentration and facilitated cofactor regeneration. The screen printed electrode casted with the hybrid system showed a wide xylose detection range of 0.5 to 10 mM or 3.33 to 66.61 mM, and a low detection limit of 0.01 mM or 3.33 mM (S/N=3), when connecting to a potentiostat or a homemade portable biosensor, respectively. The biosensor also exhibited an excellent working stability as it retained 82 % of its initial performance after 30 days. The analysis of various xylose-containing samples further revealed the merits of our portable xylose biosensor in real-time sensing, rapid response, inexpensive instrumentation, and high selectivity, suggesting its great potential in practical applications.

Introduction

Xylose, as the key monosaccharide derived from hemicellulose, one of the main constituents of lignocellulosic biomass, has been widely used in food, beverage, and pharmaceutical industries.[1-5] Recently, the need for green energy and renewable chemicals has driven the boom of biorefinery and biomanufacturing. As another abundant substrate, next to the predominant glucose, xylose has received growing attention for the production of a variety of fuels, food, and chemicals, due to the development of engineered or synthetic xylose-fed biosystems.[3, 6-9] For example, several *in vitro* enzymatic pathways have been constructed to convert xylose into inositol, hydrogen, or electricity with remarkable yields.[10-12] Additionally, the co-utilization of xylose and glucose by some non-xylose fermenting strains has emerged as an effective strategy for enhanced biomass utilization and improved biochemical production.[13] Apparently, the application and utilization of xylose plays an increasingly important role in the flourishing biorefinery and biomanufacturing. The accurate quantification of xylose, as a result, becomes highly desirable.

Several methods have been developed to detect xylose, such as high-performance liquid chromatography (HPLC),[14, 15] HPLC/mass spectrometry,[16] Raman spectroscopy[17] and near-infrared spectroscopy.[17] However, these methods usually suffer from complex processes of sample handling, long operation time, low selectivity and sensitivity, as well as expensive instrumentation. Alternatively, electrochemical sensors hold the potential to overcome these drawbacks and offer a fast, convenient, and inexpensive alternative for sugar analysis. In addition, the application of portable device coupled with electrochemical sensor could make sugar analysis more convenient, accurate and faster. Particularly, for glucose detection, biosensors based on glucose oxidase (GOx) have been commercially available for long and widely used in monitoring sugar levels in blood samples, beverages, as well as fermenters.[18, 19] On the other hand, the electrochemical biosensing of xylose is not currently available, mainly due to the lack of corresponding xylose oxidase capable of generating hydrogen peroxide or reduced electron shuttles for facile electrochemical detection. Previously, several studies were reported pertaining to the xylose biosensors based on oligosaccharide dehydrogenase,[20] aldose dehydrogenase,[21] and *Gluconobacter oxydans* whole cells.[22] Besides, non-enzymatic electrochemical sensors for xylose detection were also developed,

[a] Tianjin Institute of Industrial Biotechnology, Chinese Academy of Sciences, 32 West Seventh Avenue, Tianjin Airport Economic Area, Tianjin, 300308, P. R. China
[b] Biology Institute, Qilu University of Technology (Shandong Academy of Sciences), Key Laboratory for Biosensors of Shandong Province, 3501 Daxue Road, Changqing District, Jinan, Shandong, 250353, P. R. China
[c] School of Chemical Engineering, University of Chinese Academy of Sciences, 19A Yuquan Road, Shijingshan District, Beijing, 100049, P. R. China
[#] Equal contribution

View Article Online
DOI: 10.1039/D0AN00880J

based on pulsed amperometric detection on an electrophoretic microchip[23] or metal(oxy)hydroxide/multiwalled carbon nanotube (MWCNT)-modified electrodes.[24] To our disappointment, nearly all these sensors suffer from poor selectivity and high detection limit, resulting in overestimation and inaccuracy in xylose detection. Recently, Liu et al. developed a GOx/xylose dehydrogenase (XDH) cell surface displaying system and achieved the specific detection of xylose and glucose, respectively.[25, 26] Although the XDH (EC 1.1.1.175) used was a highly specific enzyme for xylose detection, it required the participation of NAD^+ as a cofactor, which had to be added repeatedly for each new measurement in their study. Therefore, challenges on the regeneration of liable and costly NAD^+ and its immobilization should be addressed in order to develop a xylose biosensor relying on NAD^+-dependent XDH.

Herein, a hybrid system integrating XDHs, NAD^+ and platinum nanoparticles (PtNPs)-deposited MWCNTs (PtNPs@MWCNTs) for real-time biosensing of xylose is constructed (Scheme 1). Both XDH and NAD^+ are co-immobilized on the PtNPs@MWCNTs composite, which is further coated onto the screen printed electrode (SPE) to fabricate a portable biosensor. The PtNPs@MWCNTs composite exhibits terrific electrochemical oxidation for NADH generated from xylose oxidation by XDH. Notably, the NAD^+ is conjugated with a polyethylene glycerol (PEG) arm so that it can swing back and forth between XDHs and PtNPs@MWCNTs composite with facilitated cofactor regeneration. The nanoscale rational design of this biosensor leads to a precise and sensitive detection of xylose. Furthermore, the obtained bioelectrode is demonstrated on a portable biosensor for real-time sensing of xylose-containing samples with excellent performance. This work not only provides an alternative to construct an effective real-time xylose biosensor, but also sheds light on the development of other dehydrogenase-based biosensors for versatile applications.

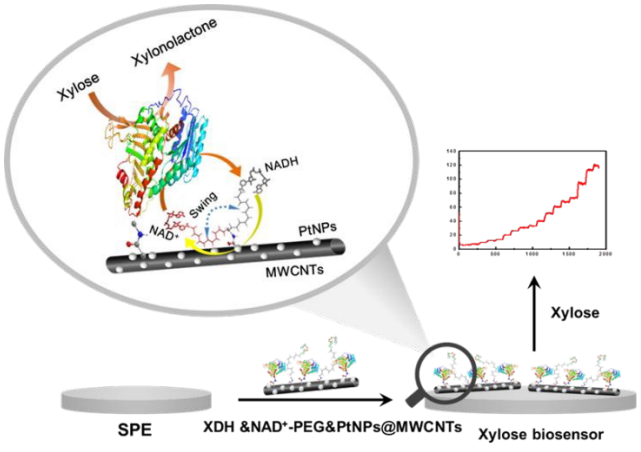

Scheme 1. Preparation of the biosensor and its sensing mechanism. PtNPs: platinum nanoparticles, MWCNTs: multiwalled carbon nanotubes, SPE: screen printed electrode, XDH: xylose dehydrogenase, PEG: polyethylene glycerol.

Experimental

Chemicals and reagents

MWCNTs were obtained from CheapTubes.com (Brattleboro, VA, USA). Chloroplatinic acid ($H_2PtCl_6{\cdot}6H_2O$) was purchased from Macklin (Shanghai, China). Ethylene glycol, NAD^+, glucose, maltose, mannose, fructose, sucrose, ribose, arabinose, galactose, xylose, polyethylene glycol-(bisamino) (NH_2-PEG-NH_2, 3000 kDa) were bought from Sigma-Aldrich (St. Louis, MO, USA). 3-Carboxyphenylboronic Acid (CBA) was purchased from Innochem (Beijing, China). N-hydroxysuccinimide (NHS) and 1-ethyl-3-(3-dimethylaminopropyl) carbodiimide hydrochloride (EDC) were from J&K Scientific (Beijing, China). SPEs were obtained from Neopro (Qingdao, China). Formate dehydrogenase (FDH) was obtained according to the previous method.[27] The phosphate buffer solution (PBS, 0.1 M) was the frequently-used buffers in the experiment. All solutions were prepared with the deionized water which was purified with a Millipore-Q purification system (18.2 MΩ cm).

Preparation of XDH

The XDH gene from *Caulobacter vibrioides* (xylB, Gene ID: 941308, NCBI) was synthesized from GenScript (Nanjing, China). The recombinant plasmid was constructed using the prolonged overlap extension polymerase chain reaction (POE-PCR). The gene was amplified with a pair of primers: 5'-TTAAC TTTAA GAAGG AGATA TACAT ATGAG CAGCG CGATC TACCC GAGCC-3' and 5'-TCAGT GGTGG TGGTG GTGGT GCTCG AGACG CCAAC CCGCA TCAAT CCAAT-3'. The plasmid pET20b was selected as the vector for recombination. The primers were 5'-ATTGG ATTGA TGCGG GTTGG CGTCT CGAGC ACCAC CACCA CCACC ACTGA-3' and 5'-GGCTC GGGTA GATCG CGCTG CTCAT ATGTA TATCT CCTTC TTAAA GTTAA-3'. *E. coli* BL21 (DE3) harboring the plasmid encoding the XDH was grown in Luria-Bertani medium supplemented with 100 μg mL^{-1} of ampicillin until the optical density at 600 nm reached ~0.6, and then the culture was incubated at 18 °C for 16 h. Cells were harvested by centrifugation and then were resuspended in 20 mM 4-(2-hydroxyethyl)-1-piperazineethanesulfonic acid (HEPES) buffer (pH 7.5) containing 50 mM NaCl. After ultrasonication, the crude enzyme was obtained via centrifugation at 4 °C and 12000 rpm for 20 min. The his-tagged XDH protein in the supernatant was further purified through the column packed with Ni-NTA resin (General Electric, NY, USA).

Preparation of PtNPs@MWCNTs composite

First, MWCNTs were activated for more carboxyl groups and enhanced solubility. Two grams of MWCNTs scattered in 20 mL HNO_3 and 60 mL H_2SO_4 were heated at 60–70 °C for 2 h, followed by a washing step to the neutral pH. The PtNPs@MWCNTs composite was synthesized by growing the PtNPs *in situ* on the surface of MWCNTs. Briefly, 50 mg MWCNTs, 10 mL 9.5 mM H_2PtCl_6 and 5 mL 40 mM KOH were added into a three-necked flask and sonicated for 30 min. Next, 25 mL ethylene glycol was added into the above-mentioned solution dropwisely under vigorous stirring for 2 h at 130 °C. The black suspension was treated by centrifugation and washed 3 times with acetone. At last, the

product was re-dispersed in ultrapure water and stored at 4 °C before use.

Fabrication of bioelectrodes

The NAD^+-PEG was prepared using a method developed by our group previously.[28] Then, 70 mM EDC and 70 mM NHS were poured into 0.5 mL 2 mg mL^{-1} PtNPs@MWCNTs composite to activate the carboxyl groups for 1 h at 25 °C. After the incubation, 55 U XDH with or without 1 mL 10 mM NAD^+-PEG was mixed with PtNPs@MWCNTs composite at 4 °C overnight to form the XDH&NAD^+-PEG&PtNPs@MWCNTs hybrid complex (Fig. S1). Next, the complex was centrifuged to remove excessive XDH and NAD^+-PEG. The unbound XDH was determined by the Bradford assay using bovine serum albumin (BSA) as a standard, while the unbound NAD^+ was quantified by measuring the absorbance change at 340 nm where NAD^+ was turned into NADH by catalysis of 10 U FDH utilizing 50 mM formate as another substrate. The reaction was carried out in a quartz cuvette and the millimolar extinction coefficients (ε) for NADH were 6.22 mM^{-1} cm^{-1}. Then the complex re-dispersed in 1 mL ultrapure water with a final concentration of 40 U mL^{-1} XDH, 6.8 mM NAD^+-PEG and 1 mg mL^{-1} PtNPs@MWCNTs. Finally, 10 μL XDH&NAD^+-PEG&PtNPs@MWCNTs hybrid complex was dropped onto the SPE. The bioelectrode was designated as XDH&NAD^+-PEG&PtNPs@MWCNTs/SPE and stored at 4 °C under a dry condition when not in use (Scheme 1).

Characterization of bioelectrodes

High resolution transmission electron microscope (HRTEM) was performed on a Tecnai G2 F30 field emission TEM instrument (FEI, Hillsboro, OR, USA) at an accelerating voltage of 80 kV. X-ray photoelectron spectroscopy (XPS) was conducted with an ESCALAB-250Xi system (Thermo Fisher Scientific, Waltham, MA, USA) using Al Kα as the X-ray source. The electrochemical impedance spectroscopy (EIS) was performed at the open circuit potential over an AC frequency range of 100 kHz to 1 Hz, with a sinusoidal perturbation of 5 mV, in order to obtain the resistance of bioelectrodes constructed. Cyclic voltammetry (CV) was measured from 0 V to 1.2 V at a scan rate of 50 mV s^{-1} using a CHI 1000C potentiostat (CH Instruments, Chenhua, China). All potentials in this work were set versus Ag/AgCl.

Preparation of a portable biosensor

The portable biosensor contained a voltage excitation circuit and an acquisition circuit (Fig. S2). In the voltage excitation circuit, the voltage of the working electrode was 0 V, converting the voltage of the K20DX256VLH7 32-bit ARM processor (Texas Instruments, Dallas, TX, USA) from 0–1.2 V to -1–1 V with IT1995 (Linear Technology Corporation, Milpitas, CA, USA) and then achieving selective amplification for the four ranges of ±1 V, ±2 V, ±5 V, ±10 V by AD8250 (Analog Devices, Cambridge, MA, USA). The output voltage of AD8250 constituted an inverting circuit through OPA227U (Texas Instruments) and then was applied to the counter electrode directly. In the acquisition circuit, two ADG441BR A/D converters (Analog Devices) could switch to the current ranges of ±1 μA, ±10 μA, ±100 μA, ±1000 μA by the amplifying resistance. The obtained -0.6–0.6 V voltage range, which was transformed from the current, was converted to 0–1.2 V by another IT1995 and used for the ARM processor.

Detection of xylose

The current generated from the XDH&NAD^+-PEG&PtNPs@MWCNTs/SPE was measured by dropping 50 μL 0.1 M PBS to the working electrode at the potential of 0.45 V with the carbon counter electrode. In addition, the XDH&NAD^+-PEG&PtNPs@MWCNTs/SPE was also applied in the portable biosensor and the current response was acquired at 0.5 V. Before xylose-containing sample was applied at room temperature, the current response was recorded as i_{p0}. After the catalytic reaction of xylose and NAD^+ at the electrode surface, the current response was recorded as i_p. The change in current was given by $\Delta i_p = i_p - i_{p0}$.

Real samples containing xylose were pretreated corncob and fermentation broth. Corncobs were collected, milled to a particle size smaller than 1 mm, and pretreated with 2% H_2SO_4, at 175 °C for 5 min. The resulting solid was mixed with H_2O and incubated at 50 °C for 2 h and then filtered. The supernatant was decolorized with 2.0% activated carbon, followed by the neutralization with $CaCO_3$ and filtration to obtain the acid-pretreated corncob sample. The fermentation broth samples were gifted by Professor Chaoguang Tian in our institute. The samples were then diluted by 10-fold (corncob) or 2-fold (fermentation broth) and subjected to the analysis. Besides measured by the portable biosensor, real samples were also quantified by high-performance liquid chromatography equipped with a Bio-Rad HPX-87H column and a refractive index detector using 5 mM H_2SO_4 as a mobile phase at 60 °C with a flow rate of 0.6 mL min^{-1}.

Results and Discussion

Morphology and electrochemical performance of PtNPs@MWCNTs composite

Fig. 1a presents the TEM image of PtNPs@MWCNTs composite. As expected, multiple black dots are clearly shown on the nanotubes with a size of 2–3 nm. The XPS image further indicates the successful construction of PtNPs@MWCNTs based on the identification of the Pt atom, C atom and O atom (Fig. 1b). Then we investigated the electrocatalytic activity of PtNPs@MWCNTs in detail. Fig. 1c shows the CV plots of NADH at various electrodes. There is no current response using a SPE or a PtNPs@MWCNTs-decorated SPE in 0.1 M PBS (black, blue). With the addition of NADH, the anodic peak potential at a bare SPE appears at 0.6 V vs Ag/AgCl (red). Notably, PtNPs@MWCNTs deposited at the SPE could reduce the overpotential of NADH oxidation, shifting the E_p value negatively by 150 mV to 0.45 V (green), and enhance the oxidation current by 2.2 folds. Of course, this enhancement would be further improved if more optimization could be performed to increase the dispersivity of PtNPs on MWCNTs. In general, this suggests that PtNPs@MWCNTs composite provides an excellent

View Article Online
DOI: 10.1039/D0AN00850J

platform for the construction of NAD^+/NADH-mediated electrochemical sensors. Additionally, to our limited knowledge, it is the first time to report that PtNPs@MWCNTs composite exhibits electrocatalytic activity for NADH and features a prominent advantage over PtNPs/polypyrrole/glassy carbon electrode (GCE),[29] poly(allylamine hydrochloride)/SPE[30] or polyaniline/Au/GCE[31] in terms of applied voltage when sensing NADH.

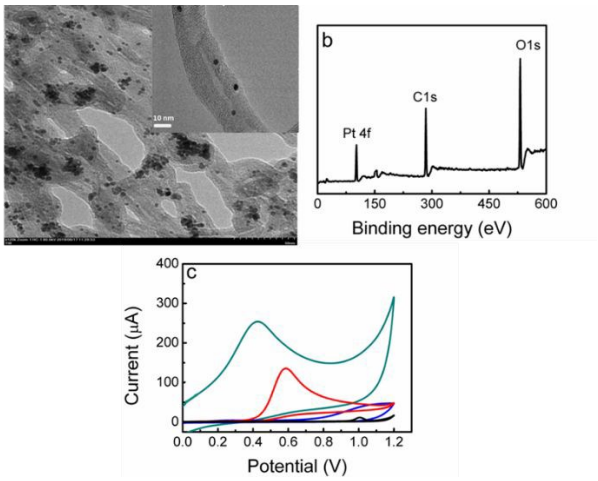

Fig. 1. (a) TEM of PtNPs@MWCNTs (The insert Fig. is the magnification); (b) XPS of PtNPs@MWCNTs; (c) CV of SPE (black, red) and PtNPs@MWCNTs/SPE (blue, green) in 0.1 M PBS (pH 7.0) (black, blue) or PBS containing 1 mM NADH (red, green).

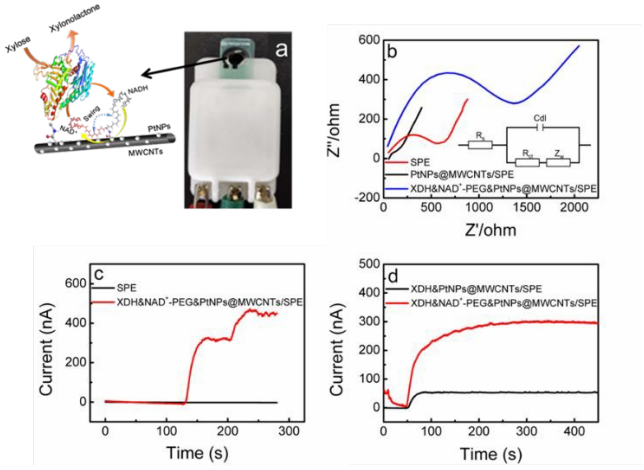

Fig. 2. (a) Photo of the XDH&NAD^+-PEG&PtNPs@MWCNTs/SPE; (b) EIS of SPE, PtNPs@MWCNTs/SPE and XDH&NAD^+-PEG&PtNPs@MWCNTs/SPE in 0.5 mM $Fe(CN)^{3+/4+}$; (c) i-t curve of SPE and XDH&NAD^+-PEG&PtNPs@MWCNTs/SPE in 0.1 M PBS with the stepwise addition of 10 mM xylose; (d) i-t curve of XDH&NAD^+-PEG&PtNPs@MWCNTs/SPE in 0.1 M PBS containing 10 mM xylose and XDH&PtNPs@MWCNTs/SPE in 0.1 M PBS with 1.36 mM NAD^+ and 10 mM xylose.

Construction of XDH&PtNPs@MWCNTs/SPE bioelectrode

XDH from *C. vibrioides* was expressed (Fig. S3a), exhibiting the enzymatic activity of ~8 U mg^{-1}. The K_m and K_{cat} of XDH for NAD^+ was 0.198 mM and 9.03 s^{-1}. The K_m and K_{cat} of XDH for xylose was 1.061 mM and 10.28 s^{-1} (Fig. S3b and S3c).[32] Then, the XDH&NAD^+-PEG&PtNPs@MWCNTs hybrid complex was casted on the SPE (Fig. 2a) and the EIS was performed to examine the immobilization result. Fig. 2b shows a Nyquist plot of different electrodes in 5 mM $K_3Fe(CN)_6/K_4Fe(CN)_6$ redox probe in 0.1 M KCl, which usually modeled by Randles's equivalent circuit.[33] The bare SPE displays a small resistance (red), while the resistance of PtNPs@MWCNTs electrode is even smaller (black), demonstrating that the latter is an excellent electrically conducting material and allows for the promotion of electron transfer. Upon the immobilization of XDH and NAD^+-PEG, an insulating protein layer was formed at the electrode surface, evident from the appearance of a significantly increased semicircular portion of the resulting spectrum (blue). This can be attributed to the block of the redox probe $Fe(CN)_6^{3-/4-}$ from reaching the electrode by immobilized XDHs and inhibited interfacial electron transfer. Apparently, the EIS result indicates a successful XDH immobilization.

Next, for the proof-of-concept of xylose response, bare SPE and XDH&NAD^+-PEG&PtNPs@MWCNTs/SPE were measured by dropping 50 μL 0.1 M PBS (pH 7.0) containing xylose. The current response at a potential of 0.45 V (vs Ag/AgCl) was captured with the stepwise addition of 10 mM xylose (Fig. 2c). The XDH&NAD^+-PEG&PtNPs@MWCNTs/SPE bioelectrode was found to generate an obvious oxidation current, illustrating the successful construction of a xylose sensing bioelectrode. In addition, we also explored the electrochemical performance of immobilized NAD^+ in the biosensor using XDH&NAD^+-PEG&PtNPs@MWCNTs/SPE and XDH&PtNPs@MWCNTs/SPE with the same loading of NAD^+-PEG, ~1.36 mM supplemented in solution. As expected, the XDH&NAD^+-PEG&PtNPs@MWCNTs/SPE bioelectrode enhanced the oxidation current nearly by 6 times compared to that of XDH&PtNPs@MWCNTs/SPE. It is caused by the fact that the immobilization of NAD^+ increases its concentration in the microenvironment surrounding XDH and PtNPs@MWCNTs composite, thus enhancing the biocatalytic efficiency and electrochemical catalytic efficiency.[27, 34]

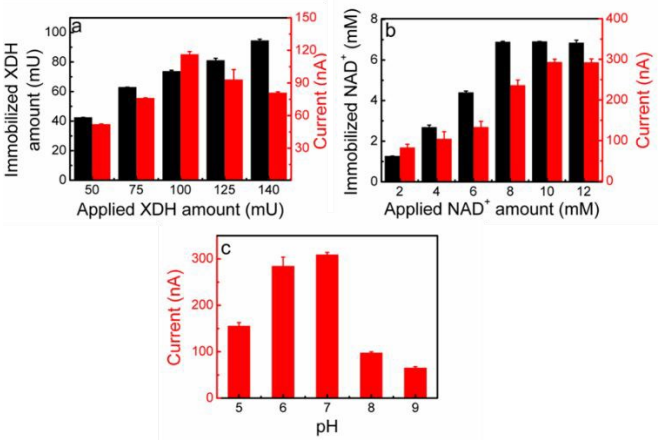

Fig. 3. (a) XDH immobilization and current response versus the applied XDH amount from 50-140 mU; (b) NAD^+ immobilization and current response versus applied NAD^+ amount from 2-12 mM; (c) Effect of pH from 5-9 on the xylose biosensing reaction.

View Article Online
DOI: 10.1039/D0AN00880J

Optimization of analytical conditions

In order to obtain a more accurate and sensitive sensing result, enzyme loading, NAD^+ loading and reaction pH were further optimized. Firstly, various loadings of XDHs from 50 mU to 275 mU were applied onto the electrodes and the unbound enzymes were rinsed away followed by Bradford assay to find out the optimal XDH loading. Fig. 3a reveals that the immobilized XDH amount increases with the applied XDH amount and their ratio is between 60% and 75%. The current response also increases with immobilized XDH amount until reaching 100 mU. More applied XDH amount reduces the current response largely due to the decrease of the conductivity of the XDH&PtNPs@MWCNTs bioelectrode as a result of more insulating protein. Secondly, various loadings of NAD^+ from 2 mM to 12 mM were applied onto the PtNPs@NMWCNTs and the unbound NAD^+ was rinsed away followed by the quantification of NADH. Fig. 3b reveals that the immobilized NAD^+ amount and current response increase with the applied NAD^+ amount. The immobilized NAD^+ amount reaches its maximum value ~6.8 mM with the applied NAD^+ amount of 8 mM and the current response is largest with the applied NAD^+ amount of 10 mM. Therefore, 10 mM NAD^+ was chosen for the preparation of the hybrid sensing system. Finally, the pH effect was investigated and an optimum value at pH 7.0 was found, in good agreement with the optimal pH reported for this XDH (Fig. 3c).

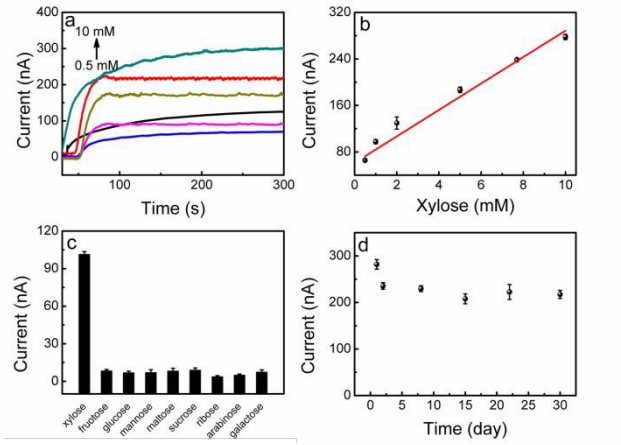

Fig. 4. (a) Corresponding current response of the biosensor in 0.1 M PBS with 0.5, 1, 2, 5, 7.7, 10 mM xylose; (b) Typical calibration plot for xylose detection using the XDH&NAD^+-PEG&PtNPs@MWCNTs/SPE bioelectrode in 0.1 M PBS with various concentrations of xylose from 0.5-10 mM; (c) Substrate specificity of the bioelectrode; (d) Stability of the bioelectrode.

Analytical performance of xylose biosensing

The oxidation current was directly related to the amount of xylose captured on the bioelectrode surface at a potential of 0.45 V. The change of the oxidation current (Δi_p) increases with the increase of xylose concentration from 0.5 mM to 10 mM (Fig. 4a and 4b). The regression equation is Δi_p=61.343+22.719c_{xylose} with a correlation coefficient of 0.985. The limit of detection (LOD) of 0.01 mM can be estimated at a signal-to-noise (S/N) ratio of 3. Additionally, we investigated the substrate selectivity of the biosensor constructed. The current response to the addition of 1 mM xylose or a series of other saccharides including maltose, mannose, glucose, fructose, sucrose, ribose, arabinose, galactose (100 mM respectively) was recorded. In contrast to xylose, other saccharides barely exhibited any current response, suggesting that there was no interference even with the presence of 100-fold excess of other substrates (Fig. 4c). The excellent specificity of the biosensor should be caused by the highly specific xylose oxidation catalysed by XDH accompanied with the reduction of NAD^+ to NADH (Scheme 1). Besides, the high catalytic activity of XDH for xylose oxidation further allows the high sensitivity of the biosensor. More gratifyingly, the current response of the biosensor still remained 82% of its initial performance after 1 month, demonstrating its favourable stability (Fig. 4d). The repeatability was estimated using five different electrodes in 0.1 M PBS containing 1 mM xylose. The relative standard deviation (RSD) was expressed as 6.5%, indicating a fairly good repeatability. Compared with other electrochemical sensors for xylose analysis, especially those with a non-specific sensing element (Table 1), our biosensor displays low LOD and excellent substrate selectivity because of the use of an enzyme sensing element. Additionally, compared with the recent biosensors using XDH displayed on cell surface as the enzyme sensing element, our biosensor co-immobilizes NAD^+ and XDH on PtNPs@MWCNTs composite as a hybrid system, overcoming the problem of repeated addition of NAD^+ and the difficulty in efficiently and stably oxidizing NADH at a overpotential of 0.45 V, lower than that of ~0.55 V or 0.7 V used in other biosensors. With the smart design, the stability of our biosensor is also better than that of others. Moreover, the detection range of our xylose biosensor is suitable for practical applications such as biomass fermentation.

A portable device for xylose analysis

To real-time measure samples via the constructed SPE, a corresponding portable biosensor mainly containing a voltage excitation circuit and an acquisition circuit was developed, allowing for the entire sensing operation and data transmission in a laptop (Fig. 5a). The oxidation current at 0.5 V linearly increases with the increasing concentration of xylose from 3.33 to 66.61 mM. The linear regression equation is Δi_p =0.470+0.134c_{xylose} with a correlation coefficient of 0.98 (Fig. 5b and 5c). The LOD is only 3.33 mM (S/N=3), possibly due to the different circuit design in the portable biosensor. Although the resulting LOD is not as good as the one measured by the electrochemical potentiostat as mentioned above, it is still much better than most xylose sensors as described in Table 1.

Analysis of real samples

We further evaluated the performance of our homemade portable biosensor based on the hybrid system by measuring the xylose content in real samples (Table 2). Corncob after an acidic pretreatment process and two fermentation broth samples were used. The samples were filtered through a 0.22 μm membrane, and the filtrate was collected and diluted with 0.1 M PBS buffer (pH 7.0) before loaded onto the bioelectrode. For comparison, HPLC was also used to measure these samples. Apparently, the results of the

View Article Online
DOI: 10.1039/D0AN00880J

Table 1. Comparison of the constructed xylose biosensor with other xylose sensors in the literature

Detection method	Sensing element	Fabrication method	LOD (mM)	Linear range (mM)	Selectivity	Stability	ref
Amperometry	Ohgosaccharlde dehydrogenase	Entrapment	-	0–1	Carbohydrates [1*]	-	[35]
Amperometry	Aldose dehydrogenase	Covalent immobilization	-	0–100	Glucose and xylose	50% after 5 days	[36]
Flow-injection system	Aldose dehydrogenase	Physical adsorption	-	0–100	Glucose and xylose	87% after 10 hours	[37]
Field effect transistor microbial sensor	Gluconobacter oxydans cells	Physical adsorption	0.5	5–30	Xylose	80% after 15 days	[38]
Amperometry	Gluconobacter oxydans cells	Physical adsorption	0.5	0–20	Xylose	60% after 35 days	[39]
Pulsed amperometry	Electrophoretic microchip	-	0.5	-	Glucose, maltose, xylose	-	[40]
Colorimetry	XDH	Displayed on cell surface	0.002	0.005–0.9	Xylose	-	[41]
Amperometry	XDH	Displayed on cell surface	0.0005	0.0006-0.1	Xylose	58% after 30 days	[42]
Cyclic voltammetry	XDH	Displayed on cell surface	0.1	0.25–4	Xylose	-	[43]
Cyclic voltammetry	Copper oxy-hydroxide/MWCNTs	-	0.006	0.2–5.0	Carbohydrates [2*]	-	[24]
Amperometry	XDH	Covalent immobilization	0.01	0.5–10	Xylose	82% after 30 days	This work

Carbohydrates [1*]: glucose, xylose, mannose, lactose, maltose, maltotriose, maltopentaose and maltohexaose

Carbohydrates [2*]: glucose, xylose, galactose and mannose

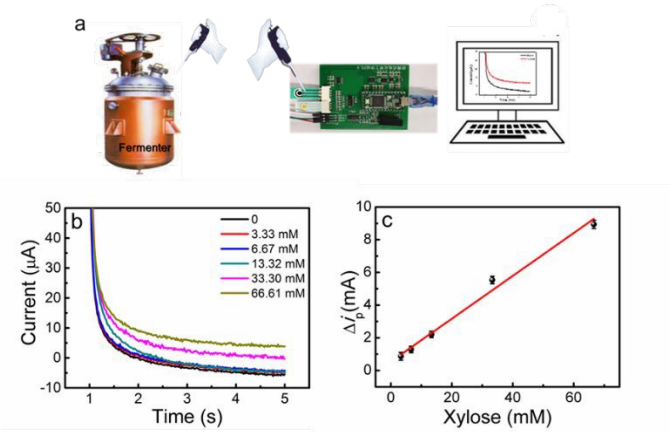

Fig. 5. (a) Working process of the portable biosensor; (b) Corresponding current response of the portable biosensor in 0.1 M PBS with 3.33-66.61 mM xylose; (c) Calibration plot for xylose detection using the portable biosensor.

Table 2. Determination of the xylose content in pretreated corncob and fermentation broth using the portable biosensor or the HPLC

	XDH&NAD$^+$-PEG&PtNPs@MWCNTs/SPE		HPLC	
	Found (mM)	RSD	Found (mM)	RSD
Corncob	12.6±0.7	5.4%	13.3±1.4	10.5%
Fermentation broth 1	17.3±1.9	10.8%	13.5±1.0	7.4%
Fermentation broth 2	42.8±2.9	6.7%	33.3±2.9	8.7%

xylose content in pretreated corncob measured by the portable biosensor and HPLC were in good agreement, illustrating that our portable biosensor was capable of precisely quantifying xylose content in real lignocellulosic samples. However, the result of fermentation broth samples had an obvious overestimation on the xylose content compared with the HPLC result. It is highly possible that the natural cofactors released by strains or contained in the medium of fermentation broth can also cause the current response. It cannot be excluded that other unknown substances may contain

View Article Online
DOI: 10.1039/D0AN00880J

NADH or its analogues which would interfere with the biosensing result as well. Albeit with this flaw of slightly overestimation when measuring complex real samples, compared with HPLC and other traditional methods, our portable xylose biosensor still features for its merits in simple operation, cheap instrumentation, rapid response, high substrate selectivity, and low LOD. Its portability further allows for the real-time sensing of samples with the minimized risk of contamination.

Conclusions

In summary, we develop a biosensor for real-time sensing of xylose based on a hybrid system. The application of XDH as the sensitive element allows for a highly sensitive and specific detection of xylose with little interference from other saccharides. The immobilization of NAD^+ coupled with a swing arm further enables the direct use of the bioelectrode without the need to add extra cofactor and enhances the current response significantly as a result of the increase of microenvironment concentration surrounding the XDH and PtNPs@MWCNTs. PtNPs@MWCNTs composite efficiently decreases the overpotential of NADH oxidation. A portable biosensor is also developed and demonstrated for real-time sensing of various xylose-containing samples. Generally, the biosensor constructed displays a wide detection range, low LOD, simple operation, inexpensive instrumentation and good storage stability, and lays a solid foundation for the practical application. Moreover, this work will be of interest to those developing other dehydrogenase and cofactor-mediated biosensors. Future efforts would be made on the increase of the recyclability of the SPE bioelectrode and the mitigation of the interference when handling with complex real samples such as the fermentation broth.

Conflicts of interest

Z.Z., H.S., and C.M. claim the financial interest to the technique disclosed in this study and have applied two Chinese patents.

Acknowledgements

This work was supported by National Natural Science Foundation of China (21878324), Natural Science Foundation of Tianjin City (19JCYBJC24600) and the CAS Pioneer Hundred Talent Program (Type C, reference # 2016-081). We gratefully thank Prof. Chaoguang Tian and Dr. Jingen Li in our institute for kindly gifting fermentation broth samples. We also thank Prof. Dong Jiang in Huazhong University of Science and Technology for revising a part of the manuscript.

Footnote

Electronic supplementary information (ESI) available.

References

1 L. Jiang, J. Wang, S. Liang, X. Wang, P. Cen and Z. Xu, *Appl. Biochem. Biotechnol.*, 2010, **160**, 350-359.
2 R. F. Perez and M. A. Fraga, *Green Chem.*, 2014, **16**, 3942-3950.
3 R. Singh, A. Shukla, S. Tiwari and M. Srivastava, *Renew. Sust. Energ. Rev.*, 2014, **32**, 713-728.
4 T. Watanabe, I. Watanabe, M. Yamamoto, A. Ando and T. Nakamura, *Bioresour. Technol.*, 2011, **102**, 1844-1848.
5 J. Zhang, A. Geng, C. Yao, Y. Lu and Q. Li, *Bioresour. Technol.*, 2012, **105**, 134-141.
6 T. Catal, K. Li, H. Bermek and H. Liu, *J. Power Sources*, 2008, **175**, 196-200.
7 L. Huang, R. J. Zeng and I. Angelidaki, *Bioresour. Technol.*, 2008, **99**, 4178-4184.
8 F. Li, Y. Li, L. Sun, X. Li, C. Yin, X. An, X. Chen, Y. Tian and H. Song, *Biotechnol. Biofuels*, 2017, **10**, 196.
9 E. M. Rubin, *Nature*, 2008, **454**, 841-845.
10 K. Cheng, W. Zheng, H. Chen and Y.-H. P. J. Zhang, *Metab. Eng.*, 2019, **52**, 1-8.
11 J. S. Martín del Campo, J. Rollin, S. Myung, Y. Chun, S. Chandrayan, R. Patiño, M. W. Adams and Y. H. P. Zhang, *Angew. Chem. Int. Ed.*, 2013, **52**, 4587-4590.
12 R. Wu, C. Ma, Y. H. P. Zhang and Z. Zhu, *ChemCatChem*, 2018, **10**, 2030-2035.
13 R. N. Avanasi, G. S. Murthy, F. W. Chaplen and C. Beatty, *Biol. Eng. Trans.*, 2013, **6**, 157-172.
14 C. Cheng, C.-S. Chen and P.-H. Hsieh, *J. Chromatogr. A*, 2010, **1217**, 2104-2110.
15 M. Raschke, M. Fellermeier and M. H. Zenk, *Anal. Biochem.*, 2004, **335**, 235-243.
16 T. Davidek, K. Kraehenbuehl, S. Devaud, F. Robert and I. Blank, *Anal. Chem.*, 2005, **77**, 140-147.
17 C.-J. Shih, J. S. Lupoi and E. A. Smith, *Bioresour. Technol.*, 2011, **102**, 5169-5176.
18 M. M. Barsan, J. Klinčar, M. Batič and C. M. Brett, *Talanta*, 2007, **71**, 1893-1900.
19 C. Sun, J. Miao, J. Yan, K. Yang, C. Mao, J. Ju and J. Shen, *Electrochim. Acta*, 2013, **89**, 549-554.
20 T. Ikeda, T. Shibata, S. Todoriki, M. Senda and H. Kinoshita, *Anal. Chim. Acta*, 1990, **230**, 75-82.
21 M. Smolander, H.-L. Livio and L. Räsänen, *Biosens. Bioelectron.*, 1992, **7**, 637-643.
22 A. N. Reshetilov, P. V. Iliasov, M. V. Donova, D. V. Dovbnya, A. M. Boronin, T. D. Leathers and R. V. Greene, *Biosens. Bioelectron.*, 1997, **12**, 241-247.
23 J. C. Fanguy and C. S. Henry, *Analyst*, 2002, **127**, 1021-1023.
24 A. C. De Sá, A. Cipri, A. González-Calabuig, N. R. Stradiotto and M. Del Valle, *Sens. Actuators B Chem.*, 2016, **222**, 645-653.
25 B. Liang, L. Li, M. Mascin and A. Liu, *Anal. Chem.*, 2012, **84**, 275-282.
26 L. Li, B. Liang, F. Li, J. Shi, M. Mascini, Q. Lang and A. Liu, *Biosens. Bioelectron.*, 2013, **42**, 156-162.
27 H. Song, C. Ma, P. Liu, C. You, J. Lin and Z. Zhu, *J CO_2 Utilization.*, 2019, **34**, 568-575.
28 H. Song, C. Ma, W. Zhou, C. You, Y.-H. P. J. Zhang and Z. Zhu, *Bioconjugate Chem.*, 2018, **29**, 3993-3998.

View Article Online
DOI: 10.1039/D0AN00880J

29 H. Mao, Y. Li, X. Liu, W. Zhang, C. Wang, S. S. Al-Deyab and M. El-Newehy, *J. Colloid Interface Sci.*, 2011, **356**, 757-762.
30 L. Rotariu, O. M. Istrate and C. Bala, *Sens. Actuactors B Chem.*, 2014, **191**, 491-497.
31 X. Feng, Y. Zhang, Z. Yan, Y. Ma, Q. Shen, X. Liu, Q. Fan, L. Wang and W. Huang, *J. Solid State Electrochem.*, 2014, **18**, 1717-1723.
32 C. Stephens, B. Christen, T. Fuchs, V. Sundaram, K. Watanabe and U. Jenal, *J. Bacteriol.*, 2007, **189**, 2181-2185.
33 Rubinstein and Israel, *J. Electrochem. Soc.*, 1987, **134**, 3078-3083.
34 H. Song, C. Ma, W. Zhou, C. You and Z. Zhu, *Bioconjugate Chem.*, 2018, **29**, 3993-3998.
35 T. S. T. Ikwda , S. Todoriki and M. Senda, *Anal. Chim. Acta*, 1990, **230**, 75-82.
36 M. Smolander, Cooper, J., Schuhmann, W., Hammerle, M., Schmidt, H.L.,, *Biosens. Bioelectron.*, 1992, **7**, 637-643.
37 J. C. M. Smolander, W. Schuhmann, M. Hammerle and H. L. Schmidt, *Anal. Chim. Acta*, 1993, **280** 119-127.
38 A. N. Reshetilov, Donova, M.V., Dovbnya, D.V., Boronin, A.M., Leathers, T.D., Greene, R.V.,, *Biosens. Bioelectron.*, 1996, **11**, 401-408.
39 P. V. I. Anatoly N. Reshetilov, Marina V. Donova, Dmitry V. Dovbnya, Alexander M. Boronin, Timothy D. Leathers b & Richard V. Greene *Biosens. Bioelectron.*, 1997, **12**, 241-247.
40 J. C. Fanguy, Henry, C.S., *Analyst*, 2002, **127**, 1021-1023.
41 B. Liang, L. Li, M. Mascin and A. Liu, *Anal. Chem.*, 2012, **84**, 275-282.
42 L. Li, B. Liang, J. Shi, F. Li, M. Mascini and A. Liu, *Biosens. Bioelectron.*, 2012, **33**, 100-105.
43 L. Li, B. Liang, F. Li, J. Shi, M. Mascini, Q. Lang and A. Liu, *Biosens. Bioelectron.*, 2013, **42**, 156-162.

View Article Online
DOI: 10.1039/D0AN00880J